Contrib Mineral Petrol (2002) 144: 22–37
DOI 10.1007/s00410-002-0382-5

Michael J. Toplis · Alexandre Corgne

An experimental study of element partitioning between magnetite, clinopyroxene and iron-bearing silicate liquids with particular emphasis on vanadium

Received: 12 December 2001 / Accepted: 30 May 2002 / Published online: 7 August 2002

Abstract Mineral-melt partition coefficients of vanadium and a series of divalent trace elements (Ni, Co, Mn, Sr) have been determined for ferrobasaltic bulk compositions at one atmosphere. Experiments were performed at constant temperature (1,068 °C) and oxygen fugacity from 0.7 log units below to 2.6 log units above the NNO buffer (NNO−0.7 to NNO + 2.6). All experiments were saturated in clinopyroxene and titanomagnetite. Partition coefficients for divalent cations between the liquid and these two minerals are found to be controlled by the ionic radius of the cation and the composition of the coexisting liquid, coefficients being significantly higher in more polymerised melts. Vanadium partitioning is strongly dependent on oxygen fugacity, decreasing by approximately one order of magnitude with increasing f_{O_2} from NNO−0.7 to NNO + 2.6 for both clinopyroxene and magnetite. Based upon thermodynamic modelling of the relative proportions of V^{3+}, V^{4+} and V^{5+} in our liquids, this behaviour is inferred to be dominated by partitioning of V^{3+}, despite the fact that this valence state is predicted to occur in low relative abundance. Derived values of $D_{V^{3+}}$ show no systematic dependence on melt polymerisation, but do show a systematic dependence on mineral composition. In particular, our data and those of the literature are combined to show that $D_{V^{3+}}^{Cpx/Liq}$ increases significantly as clinopyroxenes become more iron-rich. The partition coefficients for vanadium determined in this study have been used to model the V concentration of liquid and magnetite as a function of differentiation in a ferrobasaltic system at different oxygen fugacities. These results show that extreme enrichments of V_2O_5 in magnetite will only occur for a relatively small range of f_{O_2}, between NNO and NNO−1.5. The results of our modelling are shown to be consistent with observations made on the V-rich magnetite layers of the Bushveld intrusion.

M.J. Toplis (✉) · A. Corgne
Centre de Recherches Pétrographiques et Géochimiques,
BP 20, 54501 Vandoeuvre-lès-Nancy cedex, France
E-mail: mtoplis@crpg.cnrs-nancy.fr
Tel.: +33-383-594227
Fax: +33-383-511798

Present address: A. Corgne
Department of Earth Sciences,
Wills Memorial Building, University of Bristol,
Bristol BS8 1RJ, UK

Editorial responsibility: J. Hoefs

Introduction

Trace element abundances have long been recognised to provide important constraints on the petrogenetic processes responsible for the formation of igneous rocks (e.g. Gast 1968; Kay et al. 1970). However, it is also recognised that correct interpretation of trace element abundances requires accurate knowledge of mineral-melt partition coefficients (D), and the factors which affect them. These factors include not only the size and charge of the element of interest (e.g. Goldschmidt 1937; Onuma et al. 1968; Blundy and Wood 1994), temperature and pressure (e.g. Gast 1968; Sun et al. 1974; Green and Pearson 1983; Irvine 1987), but it is becoming increasingly clear that crystal and melt composition also play a prominent role (e.g. Blundy and Wood 1991, 1994; Kohn and Schofield 1994).

One element which has received attention in recent years is vanadium, which has the particularity that it may occur in several valence states in silicate melts at oxygen fugacities (f_{O_2}) relevant to the Earth's crust/mantle (e.g. Johnston 1965; Schreiber 1987; Carmichael and Ghiorso 1990; Hanson et al. 1996; Canil 1997; Gaetani and Grove 1997). The fact that different valence states of V are incorporated in different ways into igneous minerals results in bulk partition coefficients of V between silicate melt and coexisting minerals which are strongly dependent on f_{O_2} (Lindstrom 1976; Horn et al. 1994; Canil 1997, 1999; Canil and Fedortchouk 2000), leading to the potential for vanadium partitioning to be a redox indicator (e.g. Schreiber and Balazs 1982;

Hanson and Delano 1992; Canil 1997; Seitz et al. 1999; Brenan and Caciagli 2000; Canil 2002).

However, quantifying the exact dependence of the bulk partition coefficient of V on f_{O_2} requires complete understanding of the concentrations of different valence states of V in the melt phase as well as the factors controlling the relative magnitude of partition coefficients for individual valence states of V. With the exception of the most recent work of Canil (2002), interpretation of experimental data generally assumes that only two valence states of V coexist in the melt phase (e.g. Canil 1997) although, on thermodynamic grounds it may be shown that under certain f_{O_2} conditions, V^{3+}, V^{4+} and V^{5+} may all be present in non-negligible concentrations (Schreiber 1987; this work). The implications of this possibility on bulk partitioning behaviour have not been explored.

Furthermore, much of the previous experimental work has been oriented towards Mg-rich systems, such as komatiites (Canil 1997), and partial melting of the mantle (Canil 1999; Canil and Fedortchouk 2000). Thus, the potentially important influence of crystal and melt composition on mineral-melt partition coefficients for V have been somewhat neglected. It may be important to assess these factors, given that economically important concentrations of vanadium are associated with magnetites in Fe-rich cumulates, such as those of the Bushveld intrusion (e.g. Reynolds 1985).

The aim of the present study is thus twofold: (1) to measure and define the controls on V partitioning between titanomagnetite ($Fe_{3-x}Ti_xO_4$), clinopyroxene, and melt in Fe-bearing systems; (2) to use this information to estimate how V contents of liquids and magnetite should vary as a function of differentiation in ferrobasaltic systems, and assess under which conditions vanadium concentration will be favoured. The experiments performed for this study were also doped in a series of divalent elements. Thus, the factors affecting their distribution between melt, clinopyroxene and magnetite will also be considered.

Experimental procedure

Bulk compositions

The bulk composition chosen for this study is an evolved ferrobasalt (Mg# = 37), taken from the experimental study of Toplis et al. (1994a) and which is known to be saturated in magnetite and clinopyroxene over a wide range of f_{O_2}. A second composition was studied, identical to the first with the exception that it contains approximately 2.5 wt% P_2O_5. This choice was made because phosphorus is known to have a drastic effect on the phase relations in ferrobasaltic systems, resulting in a wide range of liquid compositions, even at fixed temperature (Toplis et al. 1994a).

The phosphorus-free starting composition was synthesised from a mixture of reagent-grade oxides (SiO_2, TiO_2, MgO, Al_2O_3 and Fe_2O_3) and carbonates ($CaCO_3$, Na_2CO_3 and K_2CO_3). This mixture was initially decarbonated in air for 30 min at ~800 °C in a thin-walled platinum crucible before complete fusion in air at ~1,300 °C for 4 h. The resulting melt was poured onto a steel plate and allowed to cool to room temperature before being finely crushed in an agate mortar under acetone. Phosphorus was added as H_3PO_4 to approximately one half of the preparation. The two powders were remelted at ~1,300 °C for a further 4 h, removed and recrushed. These glasses were then doped with approximately 3,000 ppm V, added as V_2O_5. Similar concentrations of Ni, Co, Cr, Sr and Mn were also added (as NiO, CoO, $K_2Cr_2O_7$, $SrCO_3$ and MnO_2 respectively) at this stage. The two starting compositions were then remelted in air at ~1,200 °C for 4 h, removed and recrushed once again. Chips of glass made from this powder were found to be homogeneous in composition. The level of trace element addition was chosen such that trace elements are present in sufficient concentrations to allow measurement using the electron microprobe, while remaining sufficiently dilute so that Henry's law is respected (e.g. Beattie 1993; Horn et al. 1994).

Experimental technique

The experiments were performed at atmospheric pressure in a Gero vertical drop-quench furnace (CRPG, Nancy). Temperature was controlled using an Eurotherm 818 controller and measured by two independent Pt–Pt_{10}Rh thermocouples located in the hotspot of the furnace. Thermocouple calibration was checked against the melting point of gold (1,064 °C). Oxygen fugacity was controlled using a CO–CO_2 gas mixture regulated by two Tylan mass flow controllers, fed to the furnace at low flow rate (~200 cm^3 min^{-1}) to minimise Na loss (Tormey et al. 1987). The oxygen fugacity was measured adjacent to the samples using a fixed yttrium-stabilised zirconium probe calibrated against the Ni–NiO solid buffer. During each experiment the temperature, CO gas flow rate and f_{O_2} were measured every 20 s and recorded by microcomputer.

The variations recorded show that temperature precision is better than ±1 °C and that the precision of f_{O_2} is approximately ±0.03 log units.

For each experiment ~100 mg glass powder was pressed onto a loop of platinum wire (diameter 0.2 mm), using polyvinyl alcohol as a binder. To minimise sample iron loss, all Pt loops were presaturated at the relevant f_{O_2}. Samples were introduced into the furnace in pairs (one of each composition) at a temperature above the liquidus (1,148 °C) and held for at least 9 h to allow equilibration of the multivalent ions (Fe, V). All experiments were subsequently cooled at 3 °C h^{-1} to a final temperature of 1,068 °C.

Table 1. Experimental conditions

Run[a]	D_1 (h)[b]	D_2 (h)[c]	$\log_{10} f_{O_2}$	ΔNNO[d]
AC-DEA-1	9	269	–10.06	–0.70
AC-DEA-2	12	261	–8.72	0.65
AC-DEA-4	9	121	–7.90	1.47
AC-DEA-5	9	185	–6.74	2.63

[a]For each experiment both starting compositions were simultaneously studied
[b]Dwell in hours above the liquidus (1,148 °C) to allow equilibration of the iron redox ratio before cooling
[c]Dwell in hours at the final temperature (1,068 °C)
[d]$\Delta NNO = \log_{10} f_{O_2}$ (experiment) − $\log_{10} f_{O_2}$ (NNO buffer), values of the latter calculated using Carmichael and Ghiorso (1990)

Table 2. Electron microprobe analyses of clinopyroxene, titanomagnetite and quenched liquid (wt%)

	Ph[a]	n[b]	P_2O_5	SiO_2	TiO_2	Al_2O_3	V_2O_3	Cr_2O_3	CaO	MgO	MnO	FeO*	CoO	NiO	SrO	Na_2O	K_2O	Total	XPh[c]	NBO/T[d]	D_V[e]
SC4[f]	Liq	13	–	49.5	4.3	11.5	–	–	10.0	4.8	–	14.6	–	–	–	2.9	0.48	98.08	37.0		
	1σ[g]			*0.5*	*0.2*	*0.1*			*0.1*	*0.1*		*0.4*				*0.1*	*0.03*				
P-free system																					
NNO−0.7	Mt	14	–	0.11	27.14	1.93	3.04	0.81	0.12	2.42	0.62	60.83	1.03	0.79	0.04	0.08	0.01	98.96	13.3		34.03
				0.06	*0.47*	*0.07*	*0.09*	*0.04*	*0.02*	*0.08*	*0.03*	*0.55*	*0.01*	*0.06*	*0.05*	*0.03*	*0.01*				*1.57*
	CPx	24	–	46.88	2.64	4.63	0.82	0.06	20.50	11.35	0.37	11.59	0.27	0.39	0.10	0.59	0.01	99.74	63.6		9.18
				0.85	*0.29*	*0.48*	*0.11*	*0.07*	*0.79*	*0.34*	*0.03*	*1.49*	*0.01*	*0.02*	*0.09*	*0.14*	*0.02*				*1.29*
	Liq	22	–	55.32	3.60	11.68	0.09	0.03	7.27	2.12	0.41	14.08	0.14	0.03	0.31	3.68	1.23	100.00	23.9	0.49	
				0.55	*0.46*	*1.92*	*0.00*	*0.04*	*0.71*	*0.37*	*0.04*	*0.67*	*0.00*	*0.01*	*0.06*	*0.23*	*0.03*				
NNO + 0.6	Mt	12	–	0.13	22.79	1.80	2.32	0.58	0.09	2.42	0.81	65.66	0.91	0.61	0.01	0.00	0.00	98.12	29.2		21.83
				0.05	*0.43*	*0.06*	*0.04*	*0.16*	*0.04*	*0.11*	*0.04*	*0.24*	*0.01*	*0.02*	*0.01*	*0.00*	*0.00*				*1.15*
	CPx	21	–	47.07	2.27	3.59	0.54	0.02	20.80	12.00	0.48	11.85	0.25	0.27	0.04	0.56	0.01	100.22	64.3		5.06
				0.86	*0.68*	*1.30*	*0.10*	*0.02*	*0.78*	*0.46*	*0.03*	*0.81*	*0.01*	*0.07*	*0.07*	*0.24*	*0.02*				*0.99*
	Liq	25	–	62.81	3.34	11.72	0.11	0.03	5.66	1.43	0.35	8.93	0.08	0.01	0.34	2.82	1.60	99.23	26.7	0.26	
				1.37	*0.05*	*0.39*	*0.01*	*0.04*	*0.37*	*0.19*	*0.04*	*0.37*	*0.01*	*0.00*	*0.15*	*0.07*	*0.10*				
NNO + 1.5	Mt	14	–	0.23	15.34	3.27	2.93	0.59	0.17	3.38	0.68	67.01	1.13	1.04	0.04	0.12	0.01	95.93	51.4		13.14
				0.24	*0.08*	*0.29*	*0.11*	*0.19*	*0.06*	*0.23*	*0.03*	*0.62*	*0.05*	*0.06*	*0.07*	*0.10*	*0.00*				*1.14*
	CPx	21	–	46.30	2.49	5.10	0.26	0.05	21.44	11.90	0.26	10.23	0.23	0.39	0.09	0.69	0.01	99.44	67.5		1.16
				1.15	*0.32*	*0.64*	*0.02*	*0.06*	*0.14*	*0.63*	*0.04*	*0.29*	*0.00*	*0.00*	*0.08*	*0.17*	*0.01*				*0.12*
	Liq	24	–	57.94	3.45	14.68	0.22	0.02	7.59	1.78	0.30	7.76	0.10	0.03	0.37	3.81	0.95	99.00	37.2	0.26	
				0.30	*0.10*	*0.32*	*0.02*	*0.03*	*0.17*	*0.06*	*0.02*	*0.23*	*0.01*	*0.01*	*0.09*	*0.16*	*0.07*				
NNO + 2.6	Mt	7	–	0.21	6.07	1.82	1.49	1.53	0.24	2.84	1.28	72.72	1.32	1.67	0.00	0.08	0.03	91.31	83.5		3.10
				0.26	*1.03*	*0.06*	*0.72*	*0.04*	*0.07*	*0.15*	*0.06*	*0.47*	*0.43*	*0.19*	*0.00*	*0.07*	*0.01*				*1.50*
	CPx	14	–	46.92	2.12	5.12	0.18	0.04	21.58	12.14	0.37	9.63	0.24	0.29	0.05	0.74	0.01	99.41	69.2		0.37
				1.82	*0.51*	*1.39*	*0.05*	*0.06*	*0.57*	*0.71*	*0.03*	*0.62*	*0.02*	*0.00*	*0.05*	*0.28*	*0.01*				*0.11*
	Liq	23	–	71.16	1.86	11.95	0.48	0.05	4.00	0.87	0.32	4.63	0.07	0.02	0.20	2.11	1.76	99.48	35.4	0.08	
				1.90	*0.12*	*0.72*	*0.02*	*0.06*	*0.08*	*0.18*	*0.03*	*0.28*	*0.01*	*0.01*	*0.11*	*0.47*	*0.10*				
P-bearing system																					
NNO−0.7	Mt	18	0.00	0.13	25.03	2.42	8.16	5.81	0.29	3.72	0.69	51.37	1.24	0.46	0.11	0.03	0.00	99.47	2.8		29.55
			0.00	*0.03*	*0.50*	*0.05*	*0.27*	*0.44*	*0.06*	*0.09*	*0.04*	*0.36*	*0.08*	*0.12*	*0.10*	*0.03*	*0.00*				*1.15*
	CPx	22	0.29	48.94	1.87	3.79	1.04	0.28	18.92	12.74	0.39	10.46	0.31	0.26	0.07	0.63	0.01	100.00	68.5		3.76
			0.06	*1.08*	*0.36*	*0.64*	*0.23*	*0.06*	*1.06*	*0.74*	*0.04*	*0.50*	*0.02*	*0.04*	*0.08*	*0.07*	*0.02*				*0.84*
	Liq	28	2.47	49.40	4.65	10.00	0.28	0.02	9.58	3.82	0.43	14.11	0.19	0.02	0.28	3.48	0.68	99.41	36.3	0.69	
			0.35	*0.74*	*0.21*	*0.19*	*0.01*	*0.04*	*0.32*	*0.13*	*0.02*	*0.23*	*0.01*	*0.01*	*0.16*	*0.09*	*0.06*				
NNO + 0.6	Mt	13	0.01	0.09	20.02	3.48	4.15	3.34	0.14	3.54	0.54	58.08	1.41	1.64	0.01	0.04	0.01	96.49	26.1		15.03
			0.01	*0.05*	*0.24*	*0.11*	*0.47*	*0.08*	*0.04*	*0.16*	*0.06*	*0.76*	*0.13*	*0.15*	*0.01*	*0.02*	*0.01*				*1.80*
	CPx	21	0.41	48.87	1.85	3.46	0.51	0.10	18.78	13.46	0.39	10.50	0.34	0.45	0.01	0.76	0.05	99.94	69.5		1.85
			0.27	*1.18*	*0.46*	*0.83*	*0.14*	*0.06*	*1.56*	*1.04*	*0.01*	*0.58*	*0.03*	*0.03*	*0.03*	*0.16*	*0.09*				*0.50*
	Liq	24	2.25	50.48	4.15	12.03	0.28	0.03	9.27	3.49	0.34	12.38	0.21	0.07	0.21	4.08	0.58	99.83	40.3	0.53	
			0.22	*0.51*	*0.14*	*0.20*	*0.01*	*0.04*	*0.16*	*0.09*	*0.03*	*0.35*	*0.01*	*0.00*	*0.06*	*0.12*	*0.05*				
NNO + 1.5	Mt	14	0.02	0.13	13.38	3.42	2.47	2.07	0.16	3.86	0.56	63.84	1.47	2.38	0.13	0.07	0.00	93.95	57.4		7.16
			0.04	*0.07*	*0.12*	*0.18*	*0.11*	*0.26*	*0.05*	*0.12*	*0.05*	*0.40*	*0.06*	*0.13*	*0.13*	*0.07*	*0.00*				*0.33*
	CPx	19	0.45	47.26	2.30	4.39	0.32	0.10	20.57	12.80	0.31	9.34	0.30	0.47	0.03	0.66	0.02	99.33	71.0		0.94
			0.16	*0.51*	*0.13*	*0.17*	*0.01*	*0.06*	*0.21*	*0.24*	*0.03*	*0.08*	*0.01*	*0.01*	*0.06*	*0.09*	*0.01*				*0.02*
	Liq	20	2.07	51.59	3.80	12.20	0.34	0.03	9.78	3.59	0.39	10.81	0.19	0.08	0.24	3.90	0.67	99.67	47.2	0.48	
			0.65	*0.43*	*0.12*	*0.17*	*0.00*	*0.03*	*0.10*	*0.09*	*0.04*	*0.27*	*0.00*	*0.00*	*0.14*	*0.13*	*0.08*				

NNO + 2.6	Mt	8	0.01	0.09	5.48	3.46	0.97	1.89	0.13	4.82	0.88	70.75	1.78	2.67	0.24	0.10	0.02	93.29	87.1		1.93
			0.02	*0.05*	*0.36*	*0.76*	*0.13*	*0.34*	*0.03*	*0.11*	*0.03*	*0.79*	*0.03*	*0.10*	*0.30*	*0.10*	*0.03*				*0.29*
	CPx	10	0.43	47.07	2.15	5.11	0.14	0.03	21.47	12.67	0.35	8.84	0.26	0.35	0.15	0.61	0.03	99.65	71.9		0.27
			0.13	*2.44*	*0.18*	*0.30*	*0.01*	*0.03*	*0.54*	*0.30*	*0.01*	*0.39*	*0.00*	*0.02*	*0.07*	*0.16*	*0.02*				*0.02*
	Liq	12	2.01	59.98	2.98	11.39	0.51	0.07	7.98	3.37	0.44	7.19	0.15	0.05	0.22	2.90	0.98	100.20	59.6	0.32	
			0.42	*0.83*	*0.39*	*0.69*	*0.04*	*0.07*	*0.60*	*0.33*	*0.05*	*0.70*	*0.01*	*0.01*	*0.14*	*0.23*	*0.10*				

[a]Phases: *Mt* titanomagnetite, *CPx* clinopyroxene, *Liq* quenched liquid
[b]Number of analyses
[c]Numbers represent: 100×Mg# for Liq and CPx, with $Mg\# = MgO_{mol}/(MgO_{mol} + FeO_{mol})$. FeO_{liq} calculated using Kilinc et al. (1983); 100×XMt calculated using Stormer (1983)
[d]Molar ratio of non-bridging oxygens to tetrahedrally co-ordinated cations defined by: $NBO = 2\times(MgO_{mol} + FeO_{mol} + CaO_{mol} + K_2O_{mol} + Na_2O_{mol}) + 0.25\times TiO_{2\ mol} - 2\times(Al_2O_{3\ mol} + Fe_2O_{3\ mol})$ and $T = 2\times(Al_2O_{3\ mol} + Fe_2O_{3\ mol} + P_2O_{5\ mol}) + 0.75\times TiO_{2\ mol} + SiO_{2\ mol}$. FeO_{mol} and $Fe_2O_{3\ mol}$ calculated using Kilinc et al. (1983)
[e]D_V calculated as weight ratio of V in the crystal and in the coexisting liquid
[f]P-free starting composition prior to doping
[g]Numbers in italics indicate one standard deviation of replicate analyses

Oxygen fugacities from 0.7 log units below the Ni–NiO solid buffer (NNO−0.7) to 2.6 log units above the Ni–NiO buffer (NNO + 2.6) were used (Table 1). The charges were left to equilibrate for at least 5 days before drop-quenching into water. Duration at the final temperature was sufficient to provide a close approach to equilibrium (Toplis et al. 1994a), as confirmed by the small standard deviations of multiple chemical analyses (Table 2).

A constant final temperature was chosen to eliminate this parameter as an experimental variable, thereby simplifying subsequent interpretation of the measured partition coefficients. Furthermore, at this temperature, charges contained phase proportions convenient for electron probe analyses of both titanomagnetite and clinopyroxene.

Analytical techniques

Quenched samples were lightly crushed and chips mounted in epoxy resin for electron microprobe analyses. The analyses were performed using a fully automated Cameca SX50 at the Université de Nancy I (France) and completed for Sr, Mn and Cr using a Cameca Camebax at the University of Bristol (UK). An accelerating voltage of 15 kV and a beam current of 10 nA were used for the major elements. Vanadium, Ni and Co were analysed using an accelerating voltage of 25 kV and a beam current of 100 nA, whereas Mn, Sr and Cr were analysed at 15 kV and 25 nA. Counting times of 10 s on the peak and background were used for the major elements, minor elements being analysed with a counting time of 30 s on the peak and on the background each side of the peak. Natural and synthetic minerals were used as standards for major elements. Metal, Cr_2O_3, MnO and $SrTiO_3$ were used as standards for trace elements. Incident-beam diameter was 5–10 μm on glass and 1 μm on clinopyroxene and titanomagnetite.

Results

Phase equilibria and major element compositions

The phase relations (Table 1) are in good agreement with the observations of Toplis et al. (1994a) in the undoped system. At equilibrium, each sample consists of quenched liquid (Liq), plagioclase (An_{48-58}), Ca-rich clinopyroxene (Cpx) and titanomagnetite (Mt). Whitlockite $Ca_3(PO_4)_2$ is also present at NNO + 2.6 in the P-bearing system. The only significant difference between our results and those of Toplis et al. (1994a) is that members of the hematite–ilmenite solid solution were only observed at NNO + 2.6, rather than at all oxygen fugacities, most likely due to stabilisation of Mt by the presence of Cr. As previously described by Toplis et al. (1994a), phosphorus-bearing charges contain significantly more melt than their P-free counterparts at the same f_{O_2}. Experiments under more oxidising conditions show higher proportions of clinopyroxene and titanomagnetite, except at NNO + 2.6 where the appearance of members of the hematite–ilmenite solid solution induces a decrease of the modal proportion of Mt.

One very important point to note is that despite all bulk compositions being essentially the same, the composition of the liquid in equilibrium with the crystalline phases is different in each experiment, silica contents being increasingly higher at higher f_{O_2} and low phosphorus contents (Table 2). The potential importance of these variations will be considered below. More details of

the effect of phosphorus on phase relations and mineral and melt compositions (including compositions of plagioclase and whitlockite typical of those observed in this study) can be found in Toplis et al. (1994a). As expected, titanomagnetite composition shows no dependence on P_2O_5 content but it is a strong function of f_{O_2}, as noted in numerous previous studies (e.g. Buddington and Lindsley 1964; Andersen and Lindsley 1988; Ghiorso and Sack 1991; Toplis and Carroll 1995). Clinopyroxene composition shows some variation, from Mg# 63 to 72, the Mg# following that of the liquid (see Table 2).

Partitioning of divalent elements

Experimentally determined mineral-melt partition coefficients of divalent cations ($D_{M^{2+}}$, where $M^{2+} = Ca$, Co, Ni, Mn, Mg) show no systematic dependence on oxygen fugacity (e.g. Fig. 1). In general, values of $D_{M^{2+}}$ are systematically higher for Cpx than for Mt in the same experimental charge. Furthermore, a notable feature of the data is that for a given mineral, $D_{M^{2+}}$ is systematically lower in the P-bearing liquid at fixed temperature and f_{O_2} (Fig. 1). It is also observed that D_{Ca}, D_{Co}, D_{Ni}, and D_{Mn} are generally well correlated with D_{Mg} for both Cpx and Mt (Fig. 2), pointing to a common factor controlling values of $D_{M^{2+}}$, as discussed below.

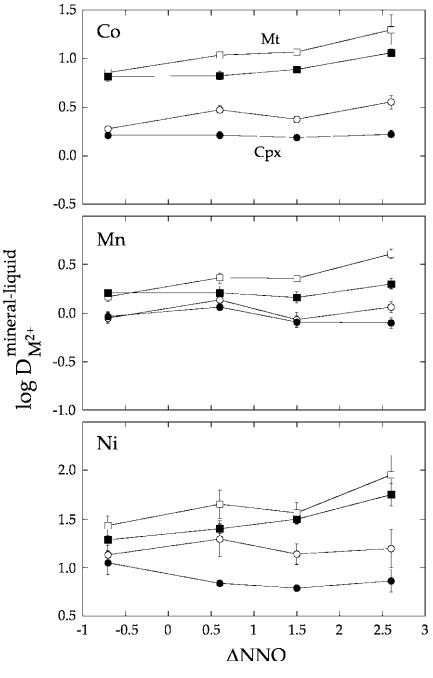

Fig. 1. Logarithm of experimentally determined mineral-melt partition coefficients of Co, Mn and Ni as a function of oxygen fugacity (expressed relative to the NNO buffer). *Squares* Liquid-titanomagnetite partition coefficients, *circles* liquid-clinopyroxene partition coefficients, *open symbols* phosphorus-free melts, *closed symbols* phosphorus-bearing melts (see text and Table 2 for more details)

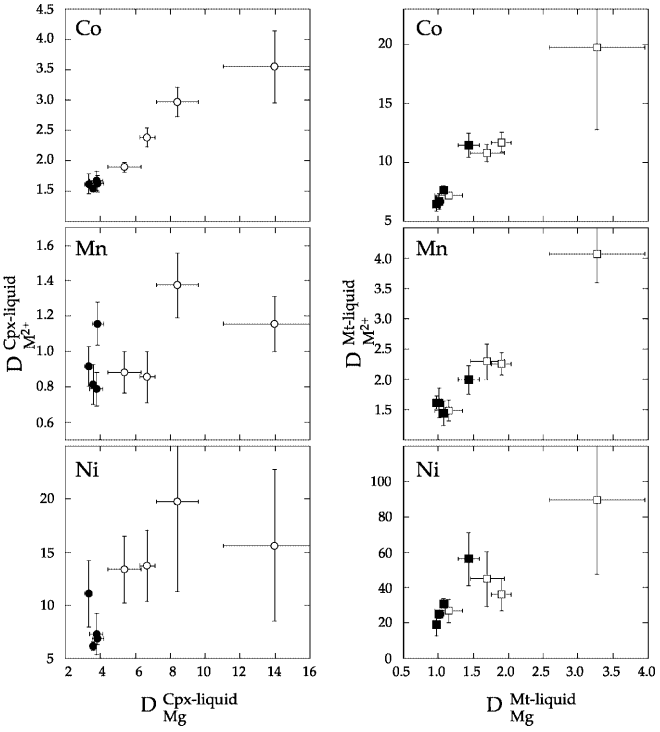

Fig. 2. Partition coefficients of Co, Mn and Ni as a function of the partition coefficient of Mg. The left-hand column (*circles*) presents data for clinopyroxene, and the right-hand column (*squares*) presents data for titanomagnetite. *Open symbols* Phosphorus-free melts, *closed symbols* phosphorus-bearing melts (see text and Table 2 for more details)

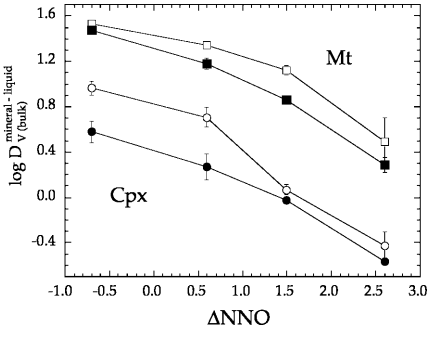

Fig. 3. Logarithm of experimentally determined bulk mineral-melt partition coefficient of V as a function of oxygen fugacity (symbols as in Fig. 1)

Vanadium partitioning

V contents in plagioclase are below the detection limit and will not be discussed further. $D_V^{Mt/Liq}$ is 4–8 times higher than $D_V^{Cpx/Liq}$ in the same experimental charge (Fig. 3; Table 2) although, as noted above for the divalent cations, both $D_V^{Mt/Liq}$ and $D_V^{Cpx/Liq}$ are systematically a factor of approximately 2 lower in the phosphorus-bearing system compared to the P-free system at the same f_{O_2} (Fig. 3; Table 2). In contrast to values of $D_{M^{2+}}$, the partition coefficient of vanadium for both Cpx

and Mt is a strong function of oxygen fugacity, decreasing by approximately one order of magnitude upon oxidation from NNO−0.7 to NNO + 2.6 (Fig. 3). To a first approximation, $\log D_V^{Mt/Liq}$ and $\log D_V^{Cpx/Liq}$ are a linear function of $\log f_{O_2}$, the average gradient of Fig. 3 varying from 0.31 to 0.43. In detail, the f_{O_2} dependence would appear to be weaker at the lowest studied oxygen fugacities (Fig. 3).

Factors controlling divalent partitioning

Crystal control: structure and composition

At fixed temperature, pressure and mineral composition, partition coefficients for suites of isovalent cations entering a particular mineral lattice site are observed to show a near parabolic dependence on ionic radius, being centred on an 'optimum radius', r_o (e.g. Onuma et al. 1968). In the case of Cpx, plots of measured $D_{M^{2+}}$ from this study (Fig. 4) may be rationalised in terms of two parabola, one defined by Ni, Mg, and Co, interpreted to represent partitioning onto the sixfold co-ordinated M1 site, the other defined by Mn, Ca and Sr, interpreted to represent partitioning onto the larger eightfold co-ordinated M2 site. Within the framework of theory linking element partitioning to crystal lattice strain (Blundy and Wood 1994), values of Young's modulus, optimum radius and optimum partition coefficient of the M1 and M2 sites may be derived from our data (see Fig. 4). These values are found to be consistent with those previously proposed in the literature (Gaetani and Grove 1995; Wood and Blundy 1997; Lundstrom et al. 1998; Hill et al. 2000). Members of the titanomagnetite solid solution also have two distinct crystallographic sites (fourfold and sixfold co-ordinated). However, data of Smyth and Bish (1988) concerning cation–O bond distances at these sites may be used to show that the optimum radius of each is relatively similar (0.66–0.68Å for the octahedral site, and 0.51–0.63Å for the tetrahedral site). The ionic radius of many divalent cations is in the same range, consistent with the fact that cations may occupy both sites (e.g. Waychunas 1991), obscuring any clear trends in partitioning behaviour as a function of ionic radius.

Variations in mineral composition may also affect partitioning behaviour due to changes in the mechanical and/or thermodynamic properties of the crystal (e.g. Blundy and Wood 1991, 1994). In the case of Cpx, major element composition varies little in our experiments, making it difficult to assess the influence of this parameter on $D_{M^{2+}}$. Even enlarging the data set to include a much wider range of Cpx compositions in systems of similar bulk composition (Toplis et al. 1994a; Toplis and Carroll 1995) does not allow us to define any simple relationship between D_{Mg}, D_{Ca}, and Mg# of Cpx, implying that in this case mineral composition is not the dominant control on the partitioning of a given divalent element. In the case of magnetite, values of $D_{M^{2+}}$ are approximately independent of f_{O_2} (Fig. 1), despite the fact that magnetite composition is a strong function of oxygen fugacity (Table 2). This observation leads us to conclude that in this case too, mineral composition is not the dominant factor affecting divalent element partitioning into magnetite–ulvöspinel solid solutions.

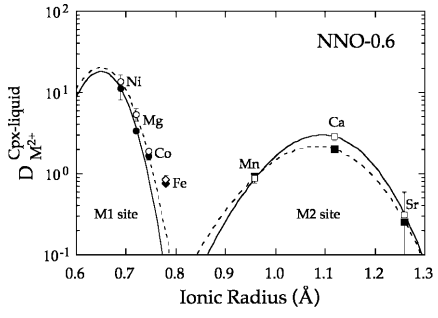

Fig. 4. Liquid-clinopyroxene partition coefficients of divalent cations as a function of ionic radius for experiments at NNO–0.6. The *solid* and *dashed lines* represent fits to Eq. (8) taken from Blundy and Wood (1994) for the clinopyroxenes in phosphorus-free and phosphorus-bearing melts respectively. Two parabola were fitted for each crystal, one corresponding to the M1 site (fitted to elements shown as *circles*), the other to the M2 site (fitted to elements shown as *squares*). The optimum radius of M1 was fixed to be 0.65Å, that for M2 being left variable. Fitted parameters for each site (optimum radius r_o, optimum partition coefficient D_o, Young's modulus E) are similar for all the clinopyroxenes modelled in this study. Typical values are: $D_oM1 = 20$, $EM1 = 1{,}250$ GPa, $r_oM2 = 1.09$Å, $D_oM2 = 2.6$, $EM2 = 180$ GPa

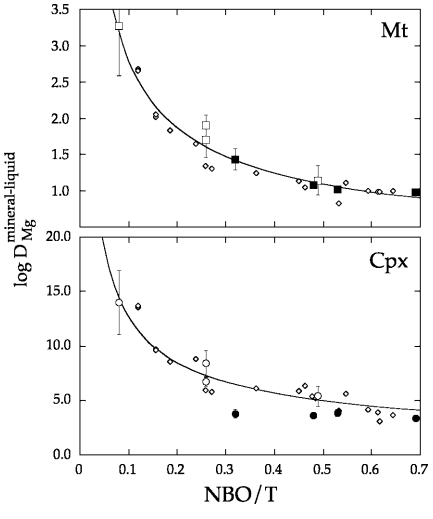

Fig. 5. Variation of the partition coefficient of Mg between mineral and liquid as a function of NBO/T, a measure of the polymerisation of the liquid (NBO/T defined in Table 2). Data from Toplis et al. (1994a) and Toplis and Carroll (1995) are also shown as *diamonds*. The *solid lines* represent fits to the equation $D_{Mg}^{Mineral/Liq} = C.(NBO/T)^{-0.58}$, where C is a constant for each mineral-element couple. The value of R^2 for the fit to $D_{Mg}^{Mt/Liq}$ is 0.96, and that for $D_{Mg}^{Cpx/Liq}$ is 0.88. As noted in the text, the data of Kohn and Schofield (1994) for partitioning of Zn between liquid and pure forsterite may also be fitted by the equation proposed above, with an R^2 value of 0.93

Influence of melt composition

When our measured values of $D_{Mg}2+$ are combined with data from Toplis et al. (1994a) and Toplis and Carroll (1995) and reported as a function of the degree of melt polymerisation (expressed by the parameter NBO/T; see Table 2 for definition), a clear trend of decreasing D_{Mg} with increasing NBO/T is apparent for both Mt and Cpx (Fig. 5). This decrease is most pronounced when NBO/T is low but it flattens off at higher values. Given the good correlation of $D_{Mg}2+$ with partition coefficients for other divalent cations (Fig. 2), it may be appreciated that the partitioning behaviour of all divalent cations shows a similar dependence on NBO/T. This variation may be qualitatively explained by the fact that melts rich in network-modifying cations contain more potential 'sites' onto which divalent cations may partition, leading to lower mineral-melt partition coefficients.

A similar dependence of partition coefficient on NBO/T has been previously described for Zn and Mn partitioning between melt and pure forsterite (Kohn and Schofield 1994). Indeed, it is highly significant that the values of $D_{M^{2+}}$ described here for magnetite and clinopyroxene, and those measured by Kohn and Schofield (1994) for olivine (of fixed composition) may all be described by the equation $\log D_{M^{2+}} = -0.58 \log (NBO/T) + C$, where C is a constant for each mineral-element pair (see Fig. 5). This observation suggests that the dependence of partition coefficient on melt polymerisation is a general feature of divalent element partitioning into many crystalline phases, and that the equation described above may be used to 'correct' divalent cation partition coefficients for the effect of liquid composition. However, we caution against application of this equation at values of NBO/T lower than 0.08, a compositional range poorly constrained by the available experimental data. We note that the difference between partition coefficients in P-bearing and P-free compositions (e.g. Fig. 1) may be simply explained by the influence of melt composition (Fig. 5), without the need to invoke a specific effect of phosphorus on partitioning behaviour.

Factors controlling vanadium partitioning

Generalities

Vanadium is unlikely to be present in the divalent state under our experimental conditions. Indeed, under conditions relevant to the Earth's crust/mantle, vanadium has been suggested to occur in silicate melts as V^{3+} and/or V^{4+} and/or V^{5+} (Johnston 1965; Schreiber 1987; Carmichael and Ghiorso 1990; Hanson et al. 1996; Gaetani and Grove 1997; Canil 1997, 2002). Assuming that one may define a distribution coefficient for each individual valence state, it may be shown that in the most general case the bulk partition coefficient between a mineral and coexisting liquid will be:

$$D_{V(bulk)}^{Mineral/Liq} = \left[XV^{3+} \times D_{V^{3+}}^{Mineral/Liq}\right] + \left[XV^{4+} \times D_{V^{4+}}^{Mineral/Liq}\right] + \left[XV^{5+} \times D_{V^{5+}}^{Mineral/Liq}\right] \quad (1)$$

where XV^{n+} is the relative concentration of V^{n+} in the liquid, and $D_{V^{n+}}^{Mineral/Liq}$ is the partition coefficient of that valence state. Consideration of Eq. (1) shows that in order to understand $D_{V(bulk)}^{Mineral/Liq}$, one must consider both the relative proportions of the various valence states of V in the melt, as well as the magnitudes of the different $D_{V^{n+}}^{Mineral/Liq}$. The concentrations of V^{n+} will be a function of the f_{O_2} and possibly the melt composition whereas, at constant temperature and pressure, $D_{V^{n+}}^{Mineral/Liq}$ may be expected to be a function of liquid and mineral composition. In the light of this complexity we will begin by considering, from a thermodynamic standpoint, the effect of f_{O_2} and melt composition on the concentrations of V^{n+}. We will then consider crystal chemical constraints on the relative magnitudes of $D_{V^{n+}}^{Mineral/Liq}$ before exploring the theoretical effect of different relative values of $D_{V^{n+}}^{Mineral/Liq}$ on the bulk partition coefficient, in particular the dependence of the latter on f_{O_2}. Only then will we consider the experimental data and attempt to quantify the different factors affecting $D_{V(bulk)}^{Mineral/Liq}$.

The redox state of vanadium in the melt phase

Effect of f_{O_2}

Because of the discrete nature of valence states, the f_{O_2} dependence of the relative proportions of reduced and oxidised members of any redox couple should be a well-defined function of f_{O_2}. For example, if vanadium were to occur as only V^{3+} and V^{4+} one may write the redox equilibrium

$$V^{3+} + 1/4\ O_2 \Leftrightarrow V^{4+} \quad (2)$$

Using standard thermodynamics, it may be shown that, at equilibrium,

$$\log\left[XV^{3+}/XV^{4+}\right] = -0.25\ \log[f_{O_2}] + \log\left[\Delta G^{o}_{(2)}\Big/2.303RT\right] - \log\left[\gamma V^{3+}/\gamma V^{4+}\right] \quad (3)$$

where XV^{n+} and γV^{n+} are the concentration and activity coefficient of V^{n+} respectively, R is the gas constant, T is temperature, and $\Delta G^{o}_{(2)}$ is the standard Gibbs free energy of equilibrium 2. Melt composition has an effect on the ratio of activity coefficients ($\gamma V^{3+}/\gamma V^{4+}$) but, if vanadium is present in trace concentrations in a matrix of fixed composition, this ratio should remain constant as a function of oxidation state. In this case, Eq. (3) may be simplified to:

$$\log\left[XV^{3+}/XV^{4+}\right] = -0.25\ \log[f_{O_2}] + E'_{(2)} \quad (4)$$

where $E'_{(2)}$ is a constant relevant to equilibrium 2, valid at fixed temperature and melt composition. The validity of Eq. (4) has been confirmed by electrochemical

measurements (e.g. Schreiber 1987) which also permit determination of E′, referred to as the 'reduction potential' (e.g. Schreiber 1987; Schreiber et al. 1999). The results of such measurements are in good agreement with independent measures of redox ratios in silicate melts, including vanadium (e.g. Schreiber and Balazs 1982; Hanson and Delano 1992; Delaney et al. 1999).

However, if V^{5+} is also present in the liquid, in addition to both V^{3+} and V^{4+}, a second redox equilibrium must be defined, for example,

$$V^{4+} + 1/4\ O_2 \Leftrightarrow V^{5+} \quad (5)$$

for which it may be shown that

$$\log[XV^{4+}/XV^{5+}] = -0.25\ \log[f_{O_2}] + E'_{(5)} \quad (6)$$

If relevant values of $E'_{(2)}$ and $E'_{(5)}$ are available, Eqs. (4) and (6) may be solved simultaneously to determine relative concentrations of the three valence states of V as a function of oxygen fugacity. As mentioned above, values of E′ for both equilibria 2 and 5 have been determined from electrochemical studies, although $E'_{(i)}$ is found to be a function of melt composition (e.g. Schreiber et al. 1994). However, despite the influence of the matrix on absolute values of E′, relative positions (i.e. $(E'_{(x)}–E'_{(y)})$ where x and y refer to two different redox equilibria) are found to be approximately constant. This is true even when the matrix changes dramatically, for example, in going from aqueous solutions to silicate melts (Schreiber et al. 1999). This result is of great importance as it implies that if E′ is known for one reference redox couple in all melts, and if $E'_{(2)}$ and $E'_{(5)}$ are known relative to that reference in at least one composition, then the values of $E'_{(2)}$ and $E'_{(5)}$ may be estimated in any melt. In melts of geological interest, the redox couple between Fe^{3+} and Fe^{2+} is an ideal reference because calculation schemes exist to predict the dependence of Fe^{2+}/Fe^{3+} on melt composition (Sack et al. 1980; Kilinc et al. 1983; Kress and Carmichael 1988), and thus to estimate E′ for the equilibrium:

$$Fe^{2+} + 1/4\ O_2 \Leftrightarrow Fe^{3+} \quad (7)$$

The case of iron in melts of geological interest may be complicated by the fact that concentrations of this element are high, resulting in variations of the ratio $\gamma Fe^{2+}/\gamma Fe^{3+}$ (and thus $E'_{(7)}$) as a function of the relative proportions of XFe^{2+} and XFe^{3+} (i.e. the oxidation state). Indeed, we believe that this effect is at the origin of the observation, embodied in the calculation scheme of Kilinc et al. (1983), that log (XFe^{2+}/XFe^{3+}) vs. $\log f_{O_2}$ has a gradient of 0.21 rather than 0.25 (Toplis, unpublished data).

For the calculation of the relative proportions of V^{n+} in composition SC4 as a function of f_{O_2} at 1,068 °C, we first define values for $E'_{(7)}–E'_{(2)}$ and $E'_{(7)}–E'_{(5)}$ from electrochemical measurements in a lime–soda glass doped with trace quantities of iron and vanadium at 1,400 °C (Schreiber et al. 1999). We then estimate $E'_{(7)}$ for composition SC4 at 1,068 °C, and the relevant f_{O_2} using the calculation scheme of Kilinc et al. (1983), from which $E'_{(2)}$ and $E'_{(5)}$ may thus be calculated (see Table 3). Values of $E'_{(2)}$ and $E'_{(5)}$ estimated in this way clearly have some associated uncertainty, but we stress that the calculated f_{O_2} dependence should be correct, and that an error in the estimated value of $E'_{(7)}$ simply displaces calculated curves (Fig. 6) by a constant amount as a function of f_{O_2}.

These calculations predict that at six log units below the NNO buffer, V^{4+} is the dominant valence state of vanadium, accounting for approximately 75% of the total V, the rest being essentially V^{3+} (Fig. 6). With increasing f_{O_2}, the relative proportion of V^{3+} falls whereas that of V^{4+} initially increases. Some increase in the proportion of V^{5+} occurs but equilibrium 2 dominates the distribution of V^{n+}. However, above NNO−3, the calculated proportion of V^{5+} begins to increase significantly, at the

Table 3. Estimated proportions of each V valence state in the melt and derived partition coefficient for V^{3+}

	$E'_{(7)}$ [a]	$\%V^{3+}_{liq}$ [b]	$\%V^{4+}_{liq}$ [b]	$\%V^{5+}_{liq}$ [b]	$D^{Cpx/Liq}_{Ti}$	$D^{Cpx/Liq}_{V^{3+}}$ [c]	$D^{Mt/Liq}_{Ti}$	$D^{Mt/Liq}_{V^{3+}}$ [c]
P-free								
NNO–0.7	–1.75	1.73	73.5	24.8	0.73	530	7.5	1,940
NNO + 0.6	–1.63	0.91	63.6	35.5	0.68	550	6.8	2,360
NNO + 1.5	–1.62	0.47	52.6	46.9	0.72	240	4.4	2,750
NNO + 2.6	–1.49	0.28	44.0	55.8	1.13	120	3.3	1,070
P-bearing								
NNO–0.7	–1.74	1.76	73.7	24.5	0.40	210	5.4	1,660
NNO + 0.6	–1.69	0.74	60.2	39.1	0.45	250	4.8	2,000
NNO + 1.5	–1.66	0.42	50.6	49.0	0.61	220	3.5	1,680
NNO + 2.6	–1.55	0.22	40.6	59.2	0.72	110	1.8	840

[a] Reduction potential for the equilibrium between ferric and ferrous iron calculated using Kilinc et al. (1983). In addition to the compositional terms given by Kilinc et al. (1983), we have added a term for 'dP_2O_5' of –6 as determined by Toplis et al. (1994b)

[b] The relative proportions of different valence states of V calculated from a combination of Eqs. (4) and (6) (see text), assuming that $E'_{(2)} = (E'_{(7)}–2.4)$, and $E'_{(5)} = (E'_{(7)}–0.3)$, the constant offsets being those determined experimentally by Schreiber et al. (1999) for a soda–lime–silicate glass

[c] Calculated partition coefficient for V^{3+} using the bulk partition coefficient shown in Table 2, the calculated proportion of V^{3+} shown in this table, and assuming a value of $D_{V^{4+}}/D_{Ti} = 0.1$, as discussed in the text

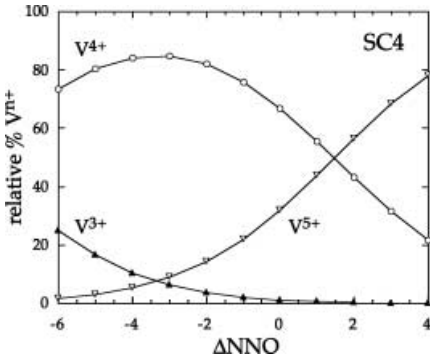

Fig. 6. Calculated variations of the relative proportions of V^{n+} as a function of oxygen fugacity for the composition SC4 (see text and Table 3 for further details)

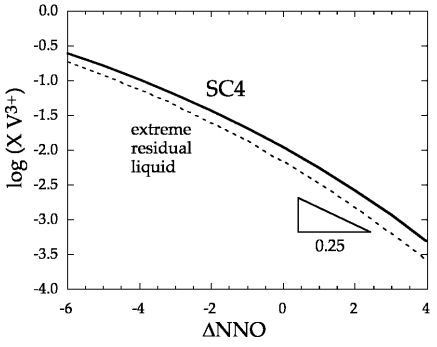

Fig. 7. Logarithm of the calculated proportion of V^{3+} as a function of the logarithm of oxygen fugacity (expressed as ΔNNO) for composition SC4 (*solid line*) and the most extreme residual liquid composition (experiment without P_2O_5 at NNO + 2.6; *dashed line*)

expense of both V^{3+} and V^{4+}, to become the dominant valence state of V at oxygen fugacities above NNO + 2 (Fig. 6). A critical feature of our calculations is that, under conditions of f_{O_2} relevant to terrestrial basaltic magmatism (NNO−3 to NNO + 1), the proportion of V^{3+} decreases, at the expense not only of V^{4+} but also increasingly of V^{5+}. This fact, reflecting the increasing role of equilibrium 5, has the consequence that the dependence of log XV^{3+} on log f_{O_2} continuously steepens with increasing f_{O_2} (Fig. 7), and may become significantly steeper than if only equilibrium 2 were active. Taking account of the simultaneous presence of V^{3+}, V^{4+} and V^{5+} in the liquid may thus be critical to the correct interpretation of the bulk partition coefficient of V, even if V^{5+} does not enter into the crystalline phases.

Melt composition

In addition to the role of f_{O_2}, a dependence of E′ on melt composition will also affect the redox state of V. For the different residual liquid compositions present in our experiments (Table 2), the magnitude of this effect may be estimated using the predicted shift of ferric-ferrous ratio as a function of melt composition, calculated using the scheme of Kilinc et al. (1983). In this calculation we have also included a term for the effect of P_2O_5, which is known to have a significant reducing effect on ferric/ferrous ratios (Toplis et al. 1994b). The calculated values of E′ are shown in Table 3 for each residual liquid composition. It is predicted that residual liquids are generally more reduced than SC4 at the same f_{O_2}, but that this effect is nevertheless minor compared to variations induced by changes in oxygen fugacity (Fig. 7).

Estimations of individual DV^{n+}

The second step to understanding the variations in $D_{V(bulk)}^{Mineral/Liq}$ is to consider the variations of D for individual valence states (Eq. 1). At first sight this may seem impossible, given that we have no direct means of measuring the relative concentrations of different valence states of V, either in the minerals or liquids. However, one possible approach is to use the observation discussed above, i.e. partition coefficients for suites of isovalent cations entering a particular mineral lattice site show a parabolic dependence on ionic radius (e.g. Onuma et al. 1968; Blundy and Wood 1994). If a suitable 'reference' cation can be identified (i.e. one which substitutes on to the same crystallographic site as vanadium), it may thus be possible to estimate $D_{V^{n+}}$ from measured values of the partition coefficient of the reference cation. We will not consider the 5+ valence state, as higher-charged cations are significantly less compatible than lower-charged cations in the same crystal and at the same site (Blundy and Wood 1994), and because there is no suitable reference 5+ cation present in all of our samples.

Site occupancies

As discussed above, the clinopyroxene crystal lattice has the general formula $M1M2T_2O_6$ where T, M1 and M2 are fourfold, sixfold, and eightfold co-ordinated cation sites of increasing optimum radius (r_o∼0.25, ∼0.65 and ∼1.0Å respectively; Gaetani and Grove 1995; Wood and Blundy 1997; Lundstrom et al. 1998; Hill et al. 2000). In light of the similarities in ionic radius between Fe^{3+} and V^{3+} in sixfold co-ordination, and between Ti^{4+} and V^{4+} in sixfold and eightfold co-ordination (Shannon 1976), it seems likely that both V^{3+} and V^{4+} may enter the M1 site of clinopyroxene, as thought to be the case for Fe^{3+} and Ti^{4+} (Gaetani and Grove 1995; Wood and Blundy 1997; Lundstrom et al. 1998; Hill et al. 2000).

In the case of the Fe–Ti oxides studied here, both magnetite ($Fe^{3+}(Fe^{2+}Fe^{3+})O_4$) and ulvöspinel ($Fe^{2+}(Ti^{4+}Fe^{2+})O_4$) have an inverse spinel structure – for a general formula AB_2O_4, cation B is present in both tetrahedral and octahedral sites, and A in an octahedral site (e.g. Wechsler et al. 1984). On the other hand, it is known that spinels containing vanadium as a major

constituent, such as coulsonite (FeV_2O_4) and vuorelainenite (MnV_2O_4), have a normal cation distribution in which cation B is located only on the octahedral site (e.g. Radkte 1962; Zakrzewski et al. 1982). This implies that V is necessarily trivalent and only occupies the octahedral site. However, when V is present in minor amounts in a titanomagnetite, V^{4+} may be present but should only enter the octahedral site because its ionic radius in fourfold co-ordination is much lower than that of the optimum radius for the tetrahedral site.

Possible reference cations

Of the trivalent cations present in our experiments, Fe^{3+} is the one which has an ionic radius closest to that of V^{3+}, making the former a potentially useful reference. However, the d^5 electronic configuration of Fe^{3+} is spherically symmetric, involving a zero crystal-field stabilisation energy (CFSE), whereas V^{3+} has a d^2 electronic configuration which is responsible for a substantial CFSE. Thus, partition coefficients may be expected to be very different, as underlined by Lindstrom (1976). Furthermore, Fe^{3+} and V^{3+} do not necessarily enter the same site, at least in magnetite. In addition, Fe^{3+} contents of both crystals and liquids have not been directly measured. Thus, $D^{Mineral/Liq}_{Fe^{3+}}$ is very poorly constrained. For all these reasons we will not pursue any comparison of $D_{V^{3+}}$ and $D_{Fe^{3+}}$.

A more promising comparison is that of V^{4+} and Ti^{4+}, which also have similar ionic radius. Although having different electronic configurations (d^0 and d^1), there is only minimal difference in their respective CFSEs. Ti^{4+} and V^{4+} may both occur exclusively on the octahedral sites of clinopyroxene and titanomagnetite. Thus, they must belong to the same partitioning parabola in each case. Applying Eq. (3) of Blundy and Wood (1994) to the case of Ti and V^{4+}, it may be shown that

$$D_{V^{4+}} = D_{Ti}\ \exp\left\{\frac{-4\pi E N_A}{RT}\left[\frac{r_o}{2}\left(r^2_{Ti} - r^2_{V^{4+}}\right) + \frac{1}{3}\left(r^3_{V^{4+}} - r^3_{Ti}\right)\right]\right\} \quad (8)$$

where E and r_o are the Young's modulus and optimum radius of the site respectively, R the gas constant, and T the temperature. Using studies of 4+ cation partitioning into the M1 site of clinopyroxene (Hart and Dunn 1993; Hauri et al. 1994; Skulski et al. 1994; Lundstrom et al. 1998; Hill et al. 2000), values for E and r_o may be estimated to be approximately 3,500 GPa (at 1,068 °C) and 0.66Å respectively. Similarly, using the studies of Smyth and Bish (1988), Horn et al. (1994), and Nielsen and Beard (2000), E and r_o for the octahedral site of magnetite can be estimated to be ~3,000 GPa and 0.67Å respectively. Using Eq. (8) and the estimated values for E and r_o, we calculate the ratio $D_{V^{4+}}/D_{Ti}$ to be approximately 0.1 for both minerals. This analysis, and measured values of D_{Ti} for each phase (Table 3) therefore imply that $D^{Mt/Liq}_{V^{4+}}$ is approximately in the range 0.1 to 1, whereas $D^{Cpx/Liq}_{V^{4+}}$ is ~0.1. We conclude that $D^{Mineral/Liq}_{V^{4+}}$ is not zero for Cpx and Mt, although the importance of $D_{V^{4+}}$ to the bulk partitioning of V will depend on the relative magnitude of $D_{V^{3+}}$, as discussed in the next section.

Effect of the relative magnitude of $D_{V^{3+}}$ and $D_{V^{4+}}$

In the literature, almost all authors working at relatively low f_{O_2} have concluded that V^{3+} is the only valence state of V incorporated into a variety of silicate and oxide minerals (e.g. Nielsen et al. 1994; Canil 1999). Evidence cited in favour of this hypothesis is the fact that the f_{O_2} dependence of bulk V partitioning is consistent with equilibrium 2 only if $D_{V^{4+}}$ is zero (Canil 1999), as well as the fact that D_V shows similarities to partitioning behaviour of other 3+ cations such as Cr^{3+} (Nielsen et al. 1994).

Given that the analysis above suggests that $D_{V^{4+}}$ is not zero, we will consider the theoretical effects of variable relative $D_{V^{3+}}$ and $D_{V^{4+}}$ on the bulk partitioning behaviour of V, assuming no role of crystal and liquid composition. We will not consider $D_{V^{5+}}$, as V partitioning studies performed under very oxidising conditions, where D_V corresponds to $D_{V^{5+}}$, show that values for the latter are very small (e.g. Horn et al. 1994; Hill et al. 2000).

When $D_{V^{3+}} >>> D_{V^{4+}}$ (approximated by $D_{V^{4+}} = 0$), $D^{Mineral/Liq}_{V(bulk)}$ should show the same f_{O_2} dependence as XV^{3+}. As illustrated in Figs. 7 and 8 for composition SC4 and $D_{V^{3+}} = 1$, this implies that the rate of change of

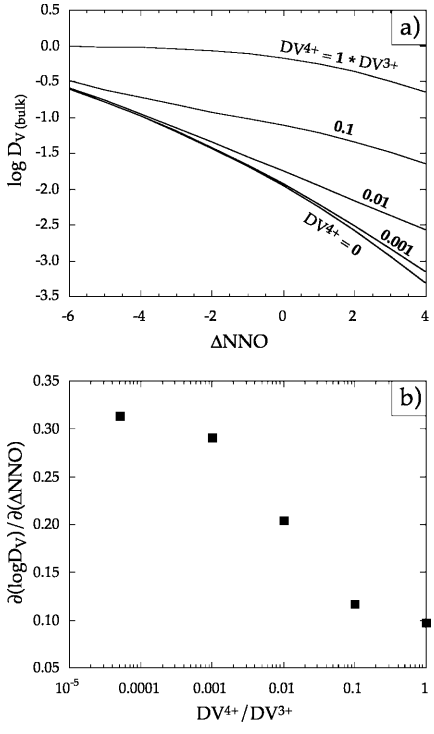

Fig. 8. **a** Calculated bulk partition coefficient of vanadium as a function of oxygen fugacity, assuming a fixed value for $D_{V^{3+}}$ of 1, and increasing relative importance of $D_{V^{4+}}$, as indicated on the figure. **b** The average gradient of **a** in the range NNO–1 to NNO + 3

$\log D_{V(bulk)}^{Mineral/Liq}$ should continuously increase to higher f_{O_2}. In the range NNO−1 to NNO + 3 (corresponding to our experimental conditions), an average gradient of 0.31 is inferred (Fig. 8b). Assuming the same value of $D_{V^{3+}}$ but increasing $D_{V^{4+}}$ to a value 0.1% that of $D_{V^{3+}}$, there is no perceptible effect on $D_{V(bulk)}^{Mineral/Liq}$, except at the highest modelled f_{O_2} (Fig. 8a), and the average gradient for our study range of f_{O_2} is only slightly affected (Fig. 8b). However, if $D_{V^{4+}}$ is increased to 1% of $D_{V^{3+}}$, there is a significant effect on the f_{O_2} dependence of predicted $\log D_{V(bulk)}^{Mineral/Liq}$ falling to a value of 0.20 (Fig. 8). Further increases of the relative magnitude of $D_{V^{4+}}$ lower the gradient of $\log D_{V(bulk)}^{Mineral/Liq}$ as a function of $\log f_{O_2}$ (Fig. 8b).

Experimental data from the literature

Before interpreting experimentally determined values of $D_{V(bulk)}^{Mineral/Liq}$, we will compare our data with those of the literature (Fig. 9a, b). This comparison confirms the strong influence of f_{O_2} on both $D_{V(bulk)}^{Mt/Liq}$ and $D_{V(bulk)}^{Cpx/Liq}$, but also shows that the absolute values of $D_{V(bulk)}^{Mineral/Liq}$ we have determined are among the highest at fixed f_{O_2}. For example, along the NNO buffer, our values for $D_{V(bulk)}^{Cpx/Liq}$ are up to one order of magnitude greater than those determined by Canil and Fedortchouk (2000) for the system Di–Ab–An, although available data for high-alumina and alkali olivine basalts, picrite, andesite, and nephelinite are generally intermediate (Fig. 9a). Another point of note is that the combined data sets of Lindstrom (1976) and Canil and Fedortchouk (2000) for the system Di–Ab–An define a single trend of $\log D_{V(bulk)}^{Cpx/Liq}$ vs. $\log f_{O_2}$ from NNO−5 to NNO + 7 which may be described by a constant gradient of 0.19, a value significantly lower than that defined by our data (Fig. 9a). For members of the spinel group, an extensive data set exists for vanadium partitioning in an alkali olivine basalt system at atmospheric pressure (Lindstrom 1976; Horn et al. 1994). These data show a coherent variation of $D_{V(bulk)}^{Mt/Liq}$ from NNO−4 to NNO + 7, with a constant gradient of 0.30 (Fig. 9b).

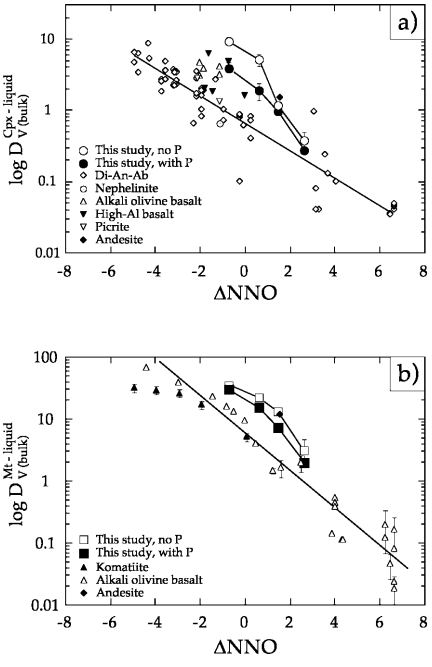

Fig. 9a, b. Comparison of our measured bulk V partition coefficients with data from the literature for **a** clinopyroxene (our data, *circles* as in Fig. 1), and **b** titanomagnetite (our data, *squares* as in Fig. 1). Literature data cover temperatures from 1,100 to 1,560 °C and pressures from 100 MPa to 2.8 GPa. Sources are Lindstrom (1976), Luhr and Carmichael (1980), Dostal et al. (1983), Ulmer (1989), Hart and Dunn (1993), Jenner et al. (1993), Hauri et al. (1994), Horn et al. (1994), Skulski et al. (1994), Canil (1999), Canil and Fedortchouk (2000), and Hill et al. (2000). Values for ΔNNO are calculated using values for the NNO buffer of Carmichael and Ghiorso (1990), and published values of f_{O_2} or values calculated based on COH equilibria at P and T (Ulmer and Luth 1991). The solid *line* not associated with our data in **a** is a linear fit to the combined data sets of Lindstrom (1976) and Canil and Fedortchouk (2000) for melts in the system Di–Ab–An, which has a gradient of 0.19 ($R^2 = 0.88$). The solid *line* in **b** is a linear fit to the combined data sets of Lindstrom (1976) and Horn et al. (1994) for alkali olivine basalts, which has a gradient 0.30 ($R^2 = 0.93$)

The relative importance of DV^{4+} and DV^{3+} in experimentally studied melts

As shown in Fig. 8, the relative magnitude of $D_{V^{3+}}$ and $D_{V^{4+}}$ may have a significant effect on the f_{O_2} dependence of $D_{V(bulk)}^{Mineral/Liq}$. We will therefore begin by considering this quantity in experimentally studied systems. If it assumed that $D_{V^{4+}}^{Mt/Liq}$ and $D_{V^{4+}}^{Cpx/Liq}$ have values 0.1 times the relevant value of D_{Ti} (as discussed above), it may be shown that for both Cpx and Mt in each of our experimental charges, $D_{V^{4+}} < 0.1\% D_{V^{3+}}$ (Table 3), consistent with the high gradients observed in Fig. 3. On the other hand, if it is assumed that $D_{V^{4+}}$ is of the same order of magnitude in all chemical systems (as suggested by a comparison of D_{Ti} measured in our experiments with results in Mg-rich systems (e.g. Skulski et al. 1994), one predicts that in the system Di–Ab–An, $D_{V^{4+}}^{Cpx/Liq}$ has a value typically 1% that of $D_{V^{3+}}^{Cpx/Liq}$. As may be appreciated from Fig. 8, this may significantly affect the f_{O_2} dependence of $D_{V(bulk)}^{Cpx/Liq}$ at high f_{O_2}. Indeed, we note that the average gradient in Fig. 9a for the combined data sets of Lindstrom (1976) and Canil and Fedortchouk (2000) for the system Di–Ab–An (0.19) is entirely consistent with the conclusions of our calculations (see Fig. 8b). Although the interpretation that vanadium partitioning is controlled exclusively by equilibrium 2 is the simplest (Canil and Fedortchouk 2000), we believe that a thermodynamically more plausible scenario is that the observed dependence of $D_{V(bulk)}^{Cpx/Liq}$ on f_{O_2} in the system Di–Ab–An is the result of the contrasting effects of a significant role of equilibrium 5, and a non-negligible $D_{V^{4+}}$ at high f_{O_2}. We underline our belief that the presence of V^{5+} in the liquid as well as the relative magnitudes of $D_{V^{3+}}$ and

$D_{V^{4+}}$ must both be taken into account when considering $D^{Mineral/Liq}_{V(bulk)}$.

Controls on $D_{V^{3+}}$

Although it is clear that the dependence of the relative proportions of XV^{n+} on f_{O_2} exerts a major control on $D^{Mineral/Liq}_{V(bulk)}$, it is of interest to try to subtract this effect and assess the factors which control $D^{Mineral/Liq}_{V^{3+}}$. To do this, we use measured $D^{Mineral/Liq}_{V(bulk)}$ coupled with calculated XV^{n+} (Table 2) and estimated DV^{4+} to calculate $D^{Mt/Liq}_{V^{3+}}$ and $D^{Cpx/Liq}_{V^{3+}}$ in our experiments (see details in Table 3). Calculated values of $D^{Mineral/Liq}_{V^{3+}}$ show some significant variation which should be the result of variations in mineral and/or melt composition. We note that although absolute values of $D^{Mineral/Liq}_{V^{3+}}$ are sensitive to $E'_{(7)}$ used for the calculation of XV^{3+}, the *trends* in $D^{Mineral/Liq}_{V^{3+}}$ described below are not.

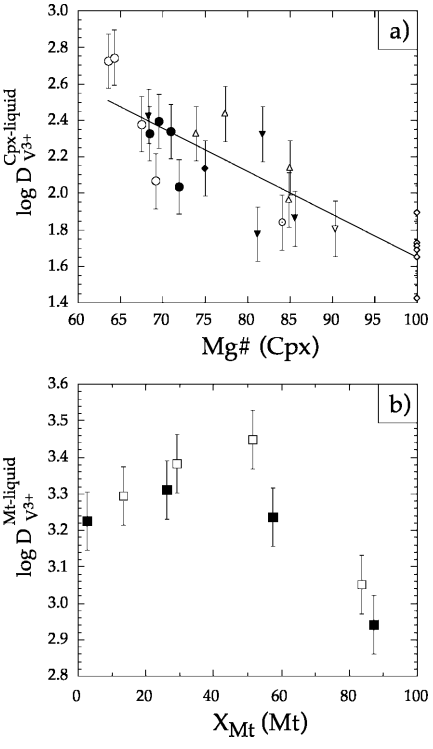

Fig. 10. **a** Calculated values of $D^{Cpx/Liq}_{V^{3+}}$ as a function of Mg# of the pyroxene. Our data are shown as large open and solid *circles*, as in Fig. 1. Literature data for which D_{Ti} could be calculated are also reported as smaller symbols. In addition, values are also shown for six experiments of Canil and Fedortchouk (2000) in an iron-free system, assuming $D^{Cpx/Liq}_{V^{4+}} = 0$. The legend for these data is the same as that for Fig. 9. The best fit to all the data (straight *line*) is defined by the equation $\log D^{Cpx/Liq}_{V^{3+}} = 3.99 - 0.0234\ Mg\#_{(Cpx)}$. **b** Calculated values of $D^{Mt/Liq}_{V^{3+}}$ as a function of XMt (calculated using Stormer 1983) for the titanomagnetites in this study (symbols as in Fig. 1). Error *bars* represent uncertainty associated with experimental sources of error only. We note that the uncertainty associated with calculated values of XV^{3+} should lead to a constant offset and not to additional dispersion in this figure

The role of melt composition has been assessed by plotting calculated $D^{Mt/Liq}_{V^{3+}}$ and $D^{Cpx/Liq}_{V^{3+}}$ as a function of NBO/T. However, neither in the case of Cpx nor Mt does any clear correlation become apparent. We therefore conclude that in contrast to the case of divalent partitioning described above (Fig. 5), melt composition does not have a major influence on vanadium partitioning in our experiments.

In contrast, when the calculated values of $D^{Cpx/Liq}_{V^{3+}}$ are plotted as a function of Mg# of the Cpx, a very clear trend appears, suggesting that $D^{Cpx/Liq}_{V^{3+}}$ increases as clinopyroxene becomes richer in iron (Fig. 10a). Indeed, comparison with values of $D^{Cpx/Liq}_{V^{3+}}$ calculated from the literature data confirm the strong dependence of $D_{V^{3+}}$ on clinopyroxene composition (Fig. 10a). Some dispersion in the data is apparent, but this may be due to uncertainties in the predicted proportion of XV^{3+} in systems of different bulk chemistry, differences in the chemistry of the Cpx (i.e. Al_2O_3 content) and/or differences in temperature. Pressure is unlikely to cause much dispersion, as discussed by Canil and Fedortchouck (2000). We note that applying the equation derived from Fig. 5 to account for a contribution of melt composition increases, rather than decreases, the dispersion in the data shown in Fig. 10a. We note that higher partition coefficients in more iron-rich members of ferromagnesian mineral solid solutions have been described previously (e.g. calcium in olivine; Jurewicz and Watson 1988; Toplis and Carroll 1995), and we suggest that this may be a general feature of element partitioning in ferromagnesian silicates.

When values of $D^{Mt/Liq}_{V^{3+}}$ calculated from our data are plotted as a function of Mt composition, a relatively well-defined variation is apparent, suggesting that the highest values of $D^{Mt/Liq}_{V^{3+}}$ occur for intermediate members of the magnetite–ülvospinel solid solution, somewhere near the 50:50 stoichiometry (Fig. 10b). Qualitatively, this variation may be understood, given that in ülvospinel-rich members incorporation of V requires energetically unfavourable coupled substitutions, whereas in magnetite-rich members there are increasing amounts of Fe^{3+} but decreasing amounts of V^{3+}, so that competition for the available sites increases. This results in higher V partition coefficients at intermediate compositions. However, we underline that this effect is relatively minor, and that for the range of Mt composition typically encountered in natural rocks, it is f_{O_2} which will have the dominant effect on the bulk partitioning of vanadium between magnetite and liquid.

Application

Vanadium enrichment in magnetites from layered intrusions

Vanadium is an element of significant economic importance, and one of its principal sources is vanadiferrous

Table 4. Mathematical constraints used for the modelling of V concentrations of liquid and magnetite as a function of differentiation (crystallisation was modelled in steps of 1 wt%, crystals being 'removed' after each crystallisation increment)

Type	Value
Temperature (T, °C) calculated from weight fraction of liquid remaining (F_L)[a]	$T(°C) = 1{,}022 + 266\times F_L - 290\times F_L^2 + 175\times F_L^3$
Relative $\%V^{3+}$ (XV^{3+}) in the liquid calculated from oxygen fugacity (expressed as ΔNNO)[b]	$\log XV^{3+} = -0.0111\times\Delta NNO^2 - 0.2916\times\Delta NNO - 1.9623$
Partition coefficient $D_{V^{3+}}^{Mt/Liq}$[b]	$10^{3.35}$
$Mg\#_{(Cpx)}$ estimated as a function of temperature (T, °C)[a]	$Mg\#_{(Cpx)} = 4.1595\times10^{-6}\times T^3 - 1.6839\times10^{-2}\times T^2 + 22.257\times T - 9{,}576.1$
Partition coefficient $D_{V^{3+}}^{Cpx/Liq}$[b]	$\log D_{V^{3+}}^{Cpx/Liq} = -0.0234 \times Mg\#_{(Cpx)} + 3.9914$
Magnetite saturation when[a]	$T(°C) < (27.2\times\Delta NNO + 1{,}125)$
Cotectic proportion (wt%): (Ol + Plag):Cpx[a]	70:30
Cotectic proportion (wt%): (Ol + Plag):Mt[a]	82:18
Cotectic proportion (wt%): (Ol + Plag):Cpx:Mt[a]	42:40:18

[a]Equations taken from fits to the experimental data of Toplis and Carroll (1995)
[b]Equations taken from fits to the data of this study

magnetites from magmatic intrusions (e.g. the Bushveld intrusion, South Africa). Even within a single magma chamber, however, not all magnetites are rich in vanadium, and thus any serious prospecting strategy requires some understanding of the conditions necessary for concentration of V. Given that our experiments have some direct bearing on this question, we have modelled the V content of liquids and magnetites during ferrobasaltic differentiation as a function of oxygen fugacity.

Seven simulations were performed for crystallisation parallel to the NNO buffer in the range NNO−2 to NNO + 1. Each simulation was performed in steps of 1 wt% crystallised, crystals being 'removed' after each crystallisation increment (i.e. an approach to perfect fractional crystallisation). Phase appearance, cotectic proportions, and the relation between % crystallised and temperature are taken from the experimental study of Toplis and Carroll (1995) for a basaltic starting composition containing 6.5 wt% MgO (information summarised in Table 4). The vanadium content of this initial liquid was fixed to be 300 ppm V, this choice being made based upon a compilation of data for over 200 MORB glasses with MgO contents in the range 6.4–6.6 wt% (RidgePet data base). It should therefore be borne in mind that although the results of these simulations provide a quantitative indication of the effect of oxygen fugacity on the behaviour of V in ferrobasaltic systems, the absolute V concentrations are only indicative. Based upon the experimental data of Toplis and Carroll (1995), olivine and plagioclase were fixed to appear at 1,170 °C and clinopyroxene at 1,130 °C in our simulations. The appearance temperature of titanomagnetite is modelled as a function of oxygen fugacity, saturating at higher temperature at higher f_{O_2} (equation shown in Table 4). The bulk partition coefficient for each phase was calculated as the product of V^{3+} in the liquid and the relevant value of $D_{V^{3+}}$. For the former, the effect of liquid composition on the relative proportions of V^{n+} was not considered, and a single equation describing the relative proportion of V^{3+} as a function of oxygen fugacity, based upon predictions for composition SC4, was used (Table 4). This choice is justified by the fact that as long as liquids remain broadly basaltic, redox equilibria are not particularly sensitive to changes in composition (Kilinc et al. 1983). A single value for $D_{V^{3+}}^{Mt/Liq}$ of $10^{3.35}$ was used, whereas $D_{V^{3+}}^{Cpx/Liq}$ was calculated for each Cpx-saturated increment using a combination of the equation shown in the legend to Fig. 10a and the variation of Mg# of the clinopyroxene as a function of temperature measured by Toplis and Carroll (1995). The calculated V

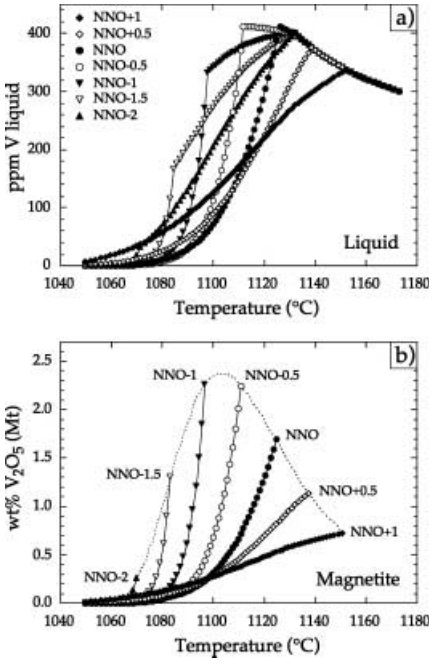

Fig. 11. **a** Calculated V content of the liquid phase (expressed as ppm V) during near-fractional crystallisation of a ferrobasaltic liquid as a function of temperature and f_{O_2}. Crystallisation was simulated in steps of 1 wt% (shown by individual symbols). The details of the calculation procedure are discussed in the text and shown in Table 4. **b** Calculated V content of magnetites (expressed as wt% V_2O_5) as a function of temperature and f_{O_2}. A symbol is placed each 1% crystallization. The thin dashed *line* is the envelope of values for the first magnetite at different oxygen fugactities

contents of the liquid and magnetite are illustrated in Fig. 11 as a function of temperature.

Before saturation in either magnetite or clinopyroxene, the vanadium content of the liquid is predicted to increase in all simulations (Fig. 11a). At the highest modelled oxygen fugacity (NNO + 1), magnetite saturation occurs before that of Cpx, leading to a gentle decrease of V in the liquid with decreasing temperature. For simulations at progressively lower f_{O_2}, the appearance of Mt is displaced to lower temperature but the subsequent depletion of the liquid in vanadium is more rapid because partition coefficients are higher (Fig. 11a). For the simulation at NNO, Cpx is predicted to saturate at slightly higher temperature than Mt. The appearance of Cpx has little effect on the V content of the liquid but the subsequent appearance of Mt rapidly depletes the liquid in V. With further decreases in f_{O_2}, even precipitation of Cpx is predicted to deplete the liquid in V (Fig. 11a), although the rate of depletion as a function of temperature increases sharply once magnetite saturates. These features lead to a somewhat unexpected behaviour of the V content of Mt as a function of f_{O_2}, with a relatively narrow f_{O_2} 'window' in which magnetites are very V-rich (Fig. 11b). At high f_{O_2} the partition coefficient of V into magnetite is low, and thus high concentrations of V do not occur. On the other hand, at low f_{O_2} the 'late' saturation of magnetite relative to Cpx has the effect that the liquid has already been depleted in V by the Cpx before Mt crystallises. Thus, in this case too, magnetites are V-poor. Only for f_{O_2} conditions between NNO and NNO−1.5 are economically important concentrations (> 1.5 wt% V_2O_5) predicted, although we recall that absolute values of V enrichment in a given intrusion will depend on the V content of the initial magma, fixed here to be 300 ppm for a magma containing 6.5 wt% MgO. One other feature of our simulations is that V concentrations in magnetite are predicted to fall very quickly as a function of continued differentiation (Fig. 11b).

Data for vanadiferrous magnetites of the Bushveld intrusion are remarkably consistent with many features of our modelling. For example, estimated f_{O_2} at the time of saturation of V-rich magnetites is in the range NNO to NNO−1 (Reynolds 1985; Cawthorn and Molyneux 1986), exactly where we predict large concentrations of vanadium (Fig. 11b). Furthermore, the highest concentration of V_2O_5 described from the base of magnetite layers is 2.23 wt% (Cawthorn and Molyneux 1986), almost identical to our predicted values. In addition, the V content of magnetites is observed to drop very rapidly as a function of stratigraphic height (Cawthorn and Molyneux 1986). The close correspondence between data for the Bushveld magnetites and our modelling of simple magmatic differentiation suggests to us that magnetite layers result from mechanical concentration of Mt, rather than a peak in oxidation (which would not lead to V-rich oxides) or the presence of an oxide-rich magma (see also discussion of Reynolds 1985; Cawthorn and Molyneux 1986).

Concluding remarks

The experimental data presented here illustrate the many factors which may affect mineral-liquid element partitioning, even at fixed temperature and pressure. In addition to differences of partition coefficient related to the size of the cation and lattice strain in the crystal (e.g. Fig. 4; Blundy and Wood 1994), we have shown that liquid composition may also play a dominant role (e.g. the case of divalent elements, Fig. 5), although this would not appear to be the case for V^{3+}. Vanadium partitioning is complicated by the presence of this element in several valence states in the liquid phase, leading to bulk partition coefficients for this element which are a strong function of oxygen fugacity (Fig. 3). Thermodynamic modelling suggests that in most geological liquids V^{3+}, V^{4+} and V^{5+} will all exist simultaneously (Fig. 6) and, although we predict that V^{3+} may be the minority valence state, we infer that it is V^{3+} which is preferentially incorporated into clinopyroxene and magnetite. Estimation of the critically important $D_{V^{3+}}^{Mineral/Liq}$ suggests that mineral composition, in particular the Mg# for clinopyroxene, has a significant effect on the partitioning behaviour of vanadium (Fig. 10a). Based upon our results, the V content of liquids and magnetite has been simulated as a function of temperature and oxygen fugacity. The results of these simulations are qualitatively consistent with observations made on the vanadiferrous magnetite seams of the Bushveld intrusion. However, detailed modelling of the behaviour of vanadium during crystallisation of layered intrusions (e.g. the Skaergaard intrusion, see Jang et al. 2001) will require further work, in particular the determination of ilmenite-liquid partition coefficients.

Acknowledgements This work is CRPG contribution number 1584. It was financially supported in part by l'Institut National des Sciences de l'Univers (programme Intérier de la Terre, contribution number 317). Grant Cawthorn and an anonymous reviewer are thanked for their comments, and JE Mungall for discussions during the early stages of this work. The help of the technical staff at the Service Commun de Microanalyse at Nancy University is also acknowledged.

References

Andersen DJ, Lindsley DH (1988) Internally consistent solution models for Fe-Mg-Mn-Ti oxides: Fe-Ti oxides. Am Mineral 73:714–726

Beattie P (1993) On the occurrence of apparent non-Henry's Law behaviour in experimental partitioning studies. Geochim Cosmochim Acta 57:47–55

Blundy JD, Wood BJ (1991) Crystal-chemical controls on the partitioning of Sr and Ba between plagioclase feldspar, silicate melts, and hydrothermal solutions. Geochim Cosmochim Acta 55:193–209

Blundy J, Wood B (1994) Prediction of crystal-melt partition coefficients from elastic moduli. Nature 372:452–454

Brenan JM, Caciagli NC (2000) Fe-Ni exchange between olivine and sulphide liquid: Implications for oxygen barometry in sulphide-saturated magmas. Geochim Cosmochim Acta 64:307–320

Buddington AF, Lindsley DH (1964) Iron-titanium oxide minerals and synthetic equivalents. J Petrol 5:310–357

Canil D (1997) Vanadium partitioning and the oxidation state of Archean komatiite magmas. Nature 389:842–845

Canil D (1999) Vanadium partitioning between orthopyroxene, spinel and silicate melt and the redox states of mantle source regions for primary magmas. Geochim Cosmochim Acta 63:557–572

Canil D (2002) Vanadium in peridotites, mantle redox and tectonic environments: Archean to present. Earth Planet Sci Lett 195:75–90

Canil D, Fedortchouk Y (2000) Clinopyroxene-liquid partitioning for vanadium and the oxygen fugacity during formation of cratonic and oceanic mantle lithosphere. J Geophys Res 105:26003–26016

Carmichael ISE, Ghiorso MS (1990) Controls on oxidation-reduction relations in magmas. Mineralogical Society of America, Washington, DC, Rev Mineral 24:191–212

Cawthorn RG, Molyneux TG (1986) Vanadiferous magnetite deposits of the Bushveld Complex. In: Anhaeusser CR, Maske S (eds) Mineral deposits of southern Africa. Geol Soc S Afr, pp 1251–1266

Delaney JS, Sutton SR, Newville M, Jones JH, Hanson B, Dyar MD, Schreiber H (1999) Synchrotron micro-XANES measurements of vanadium oxidation state in glasses as a function of oxygen fugacity: experimental calibration of data relevant to partition coefficient determination. Lunar Planet Sci XXXI:1806

Dostal J, Dupuy C, Carron JP, Le Guen de Kerneizon M, Maury RC (1983) Partition coefficients of trace elements: Application to volcanic rocks of St. Vincent, West Indies. Geochim Cosmochim Acta 47:525–533

Gaetani GA, Grove TL (1995) Partitioning of rare earth elements between clinopyroxene and silicate melt: crystal-chemical control. Geochim Cosmochim Acta 59:1951–1962

Gaetani GA, Grove TL (1997) Partitioning of moderately siderophile elements among olivine, silicate melt, and sulphide melt: Constraints on core formation in the earth and Mars. Geochim Cosmochim Acta 61:1829–1846

Gast PW (1968) Trace element fractionation and the origin of tholeiitic and alkaline magma types. Geochim Cosmochim Acta 32:1057–1086

Ghiorso MS, Sack RO (1991) Fe-Ti oxide geothermometry: thermodynamic formulation and the estimation of intensive variables in silicic magmas. Contrib Mineral Petrol 108:485–510

Goldschmidt VM (1937) The principles of distribution of chemical elements in minerals and rocks. J Chem Soc 1:655–673

Green TH, Pearson NJ (1983) Effects of pressure on rare earth element partition coefficients in common magmas. Nature 305:414–416

Hanson BZ, Delano JW (1992) Experimental data bearing on the oxidation state of chromium and vanadium in mafic volcanics. Lunar Planet Sci XXIII:481–482

Hanson BZ, Jones JH, Gaetani GA (1996) Partition coefficients for Cr^{2+} and Cr^{3+} between olivine and liquid are virtually identical: Cr and V partitioning among olivine, spinel and silicate liquid over a wide range of fO_2's. EOS Trans Am Geophys Union 77:846

Hart SR, Dunn T (1993) Experimental cpx/melt partitioning of 24 trace elements. Contrib Mineral Petrol 113:1–8

Hauri EH, Wagner TP, Grove TL (1994) Experimental and natural partitioning of Th, U, Pb and other trace elements between garnet, clinopyroxene and basaltic melts. Chem Geol 117:149–166

Hill E, Wood BJ, Blundy JD (2000) The effect of Ca-Tschermaks component on trace element partitioning between clinopyroxene and silicate melt. Lithos 53:203–215

Horn I, Foley SF, Jackson SE, Jenner GA (1994) Experimentally determined partitioning of high field strength and selected transition elements between spinel and basaltic melts. Chem Geol 117:194–218

Irvine TN (1987) Processes involved in the formation and development of layered igneous rocks. In: Parsons I (ed) Origin of igneous layering. D Reidel, Dordrecht, pp 649–656

Jang YD, Naslund HR, McBirney AR (2001) The differentiation trend of the Skaergaard intrusion and the timing of magnetite crystallizaton: iron enrichment revisited. Earth Planet Sci Lett 189:189–196

Jenner GA, Foley SF, Jackson SE, Green TH, Fryer BJ, Longerich HP (1993) Determination of partition coefficients for trace elements in high pressure-temperature experimental run products by laser ablation microprobe-inductively coupled plasma-mass spectrometry (LAM-ICP-MS). Geochim Cosmochim Acta 58:5099–5103

Johnston WD (1965) Oxidation-reduction equilibria in molten Na_2O-$2SiO_2$ glass. J Am Ceram Soc 48:184–190

Jurewicz AJG, Watson EB (1988) Cations in olivine, part 1. Calcium partitioning and calcium-magnesium distribution between olivines and coexisting melts with petrological applications. Contrib Mineral Petrol 99:176–185

Kay R, Hubbard NJ, Gast PW (1970) Chemical characteristics and origin of oceanic ridge volcanic rocks. J Geophys Res 75:1585–1613

Kilinc A, Carmichael ISE, Rivers ML, Sack RO (1983) The ferric-ferrous ratio of natural silicate liquids equilibrated in air. Contrib Mineral Petrol 83:136–140

Kohn SC, Schofield PF (1994) The importance of melt composition in controlling trace-element behaviour: an experimental study of Mn and Zn partitioning between forsterite and silicate melts. Chem Geol 117:73–87

Kress VC, Carmichael ISE (1988) Stoichiometry of the iron oxidation reaction in silicate melts. Am Mineral 73:1267–1274

Lindstrom DJ (1976) Experimental study of the partitioning of the transition metals between clinopyroxene and coexisting silicate liquids. PhD Thesis, University of Oregon, Eugene

Lundstrom CC, Shaw HF, Ryerson FJ, Williams Q, Gill J (1998) Crystal chemical control of clinopyroxene-melt partitioning in the Di-Ab-An system: Implications for elemental fractionations in the depleted mantle. Geochim Cosmochim Acta 62:2849–2862

Luhr JF, Carmichael ISE (1980) The Colima volcanic complex, Mexico. Contrib Mineral Petrol 71:343–372

Nielsen RL, Beard JS (2000) Magnetite-melt HFSE partitioning. Chem Geol 164:21–34

Nielsen RL, Forsythe LM, Gallahan WE, Fisk MR (1994) Major- and trace element magnetite-melt equilibria. Chem Geol 117:167–191

Onuma N, Higuchi H, Wakita H, Nagasawa H (1968) Trace element partitioning between two pyroxene and the host lava. Earth Planet Sci Lett 5:47–51

Radkte AS (1962) Coulsonite, FeV_2O_4, a spinel-type mineral from Lovelock, Nevada. Am Mineral 47:1284–1291

Reynolds IM (1985) The nature and origin of titanomagnetite-rich layers in the upper zone of the Bushveld Complex: a review synthesis. Econ Geol 80:1089–1108

Sack RO, Carmichael ISE, Rivers M, Ghiorso MS (1980) Ferric-ferrous equilibria in natural silicate liquids at 1 bar. Contrib Mineral Petrol 75:369–376

Schreiber HD (1987) An electrochemical series of redox couples in silicate melts: a review and applications to geochemistry. J Geophys Res 92:9225–9232

Schreiber HD, Balazs GB (1982) Vanadium as an oxygen geobarometer in basaltic magmas: The further development of a geochemical electromotive force series. Lunar Planet Sci XIII:692–693

Schreiber HD, Kochaniwski BK, Schreiber CW, Morgan AB, Coolbaugh MT, Dunlap TG (1994) Compositional dependence of redox equilibria in sodium-silicate glasses. J Non-Crystall Solids 177:340–346

Schreiber HD, Wilk NR, Schreiber CW (1999) A comprehensive electromotive force series of redox couples in soda-lime-silicate glass. J Non-Crystall Solids 253:68–75

Seitz HM, Altherr R, Ludwig T (1999) Partitioning of transition elements between orthopyroxene and clinopyroxene in peridotitic and websteritic xenoliths: New empirical geothermometers. Geochim Cosmochim Acta 63:3967–3982

Shannon RD (1976) Revised effective ionic radii in halides and chalcogenides. Acta Crystallogr A32:751–767

Skulski T, Minarik W, Watson EB (1994) High-pressure experimental trace-element partitioning between clinopyroxene and basaltic melts. Chem Geol 117:127–147

Smyth JR, Bish DL (1988) Crystal structures and cation sites of the rock-forming minerals. Allen & Unwin, Boston

Stormer JC Jr (1983) The effects of recalculation on estimates of temperature and oxygen fugacity from analyses of multicomponent iron-titanium oxides. Am Mineral 68:586–594

Sun CO, Williams RJ, Sun SS (1974) Distribution coefficients of Eu and Sr for plagioclase-liquid equilibria in oceanic ridge basalt: an experimental study. Geochim Cosmochim Acta 38:1415–1433

Toplis MJ, Carroll MR (1995) An experimental study of the influence of oxygen-fugacity on Fe-Ti oxide stability, phase relations, and mineral-melt equilibria in ferro-basaltic systems. J Petrol 36:1137–1170

Toplis MJ, Libourel G, Carroll MR (1994a) The role of phosphorus in the crystallization processes of basalt: an experimental-study. Geochim Cosmochim Acta 58:797–810

Toplis MJ, Dingwell DB, Libourel G (1994b) The effect of phosphorus on the iron redox ratio, viscosity, and density of an evolved ferro-basalt. Contrib Mineral Petrol 117:293–304

Tormey DR, Grove TL, Bryan WB (1987) Experimental petrology of normal MORB near the Kane Fracture Zone: 220–250 N, mid-Atlantic ridge. Contrib Mineral Petrol 96:121–139

Ulmer P (1989) Partitioning of high field strength elements among olivine, pyroxenes, garnet and calc-alkaline picrobasalt: experimental results and application. Carnegie Inst Washington Yearb 88:42–47

Ulmer P, Luth RW (1991) The graphite-COH fluid equilibrium in P,T,fO_2 space: an experimental determination to 30 kbar and 1600 °C. Contrib Mineral Petrol 106:265–272

Waychunas GA (1991) Crystal chemistry of oxides and oxyhydroxides. In: Lindsley DH (ed) Oxide minerals: Petrologic and magnetic significance. Rev Mineral 25:11–68

Wechsler BA, Lindsley DH, Prewitt CT (1984) Crystal structure and cation distribution in titanomagnetites ($Fe_{3-x}Ti_xO_4$). Am Mineral 69:754–770

Wood BJ, Blundy JD (1997) A predictive model for rare earth element partitioning between clinopyroxene and anhydrous silicate melt. Contrib Mineral Petrol 129:166–181

Zakrzewski MA, Burk EAJ, Lustenhouwer WJ (1982) Vuorelainenite, a new spinel and associated minerals from Satra (Doverstorp) pyrite deposit central Sweden. Can Mineral 20:281–290